LASER INTERFEROMETER GRAVITATIONAL WAVE OBSERVATORY
- LIGO -
CALIFORNIA INSTITUTE OF TECHNOLOGY
MASSACHUSETTS INSTITUTE OF TECHNOLOGY

LIGO-xxxxxxx-xx-x 2012/07/13

GEO Squeezing Noise Budget

Kate Dooley, Hartmut Grote, Henning Vahlbruch (*alphabetical order for now*)

Distribution of this document:

LIGO Scientific Collaboration

Draft

California Institute of Technology
LIGO Project, MS 18-34
Pasadena, CA 91125
Phone (626) 395-2129
Fax (626) 304-9834
E-mail: info@ligo.caltech.edu

Massachusetts Institute of Technology
LIGO Project, Room NW17-161
Cambridge, MA 02139
Phone (617) 253-4824
Fax (617) 253-7014
E-mail: info@ligo.mit.edu

LIGO Hanford Observatory
Route 10, Mile Marker 2
Richland, WA 99352
Phone (509) 372-8106
Fax (509) 372-8137
E-mail: info@ligo.caltech.edu

LIGO Livingston Observatory
19100 LIGO Lane
Livingston, LA 70754
Phone (225) 686-3100
Fax (225) 686-7189
E-mail: info@ligo.caltech.edu

http://www.ligo.caltech.edu/

1 Introduction

This document serves as a summary of the current understanding of the noise budget of the GEO squeezer. It includes the following:

- overview of the GEO squeezer setup
- review of mechanisms by which the squeezing level as seen in h is affected
- description of methods and results of measurements of the optical losses and phase noise
- design and characterization of the control loops that intregrate the squeezer with the interferometer
- suggestions for future work

2 Overview of squeezing setup

A description of the GEO squeezer itself can be found in Ref. [Henning's 2010 Class. Quantum Grav. paper]. Coherent control sidebands, Faraday isolator injection point, ...

3 Reductions to potential squeezing

The amount of squeezing that can be achieved with an interferometer is a function of three primary quantities:

1. level of injected squeezing
2. optical losses (including mode-matching and alignment)
3. phase noise

Models are presented here and measurements follow in the next sections.

3.1 Injected squeezing

The level of injected squeezing is limited to the performance of the squeezer itself. In day-to-day activities, we adjust the level of squeezing generated by the squeezer by changing

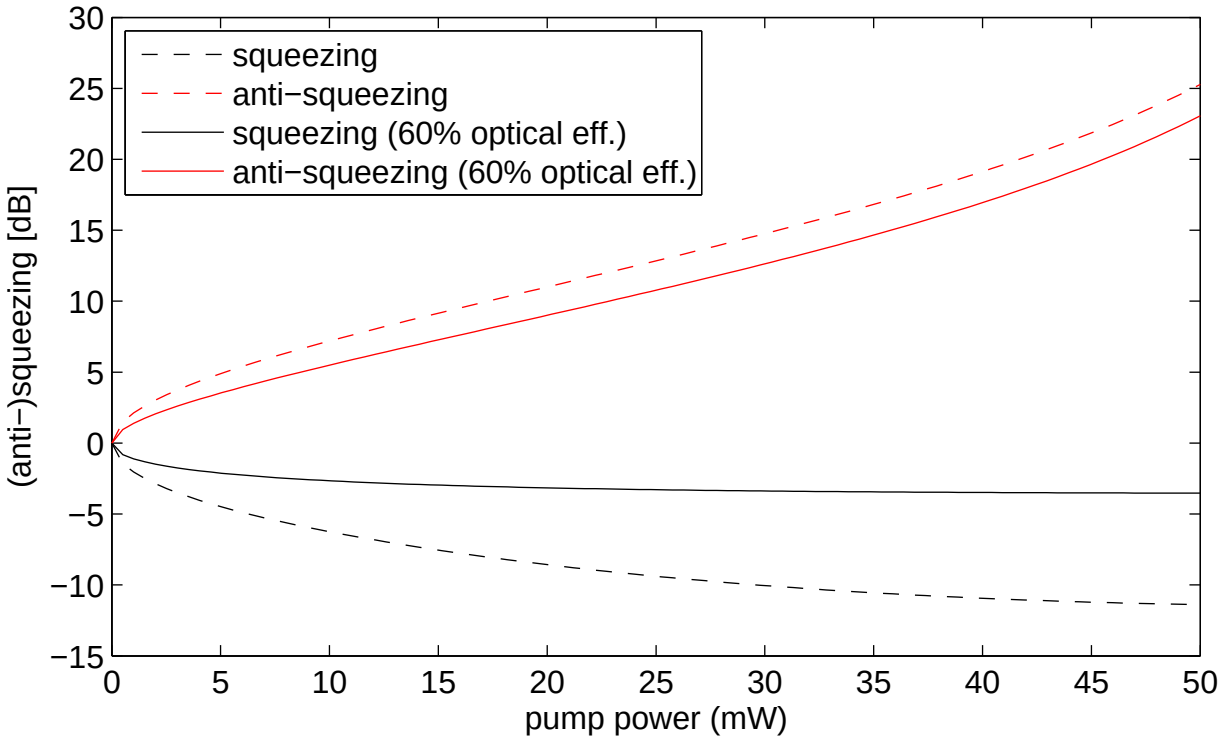

Figure 1: The amount of generated squeezing and anti-squeezing as a function of the green pump power. An example of the effect of optical losses is included by showing the equivalent curves when the optical efficiency of the squeezer path is 60%. No phase noise is included. compare pump power to non-linear gain; which is most general?

the setpoint for the Mach-Zehnder (MZ). A PZT on one of the MZ mirrors changes the MZ length and therefore controls the amount of green light transmitted through the MZ to match the requested setpoint. This green pump field is sent directly into the OPA cavity to generate the correlated 1064 nm photons. The degree of squeezing is a non-linear function of the pump power and is plotted in Figure 1 using the GEO squeezer parameters which are found in Table 1. This shows the upper limits of our achievable squeezing level. A maximum pump power of 45 mW, or 11 dB of generated squeezing, may be used with the GEO squeezer.

Table 1: GEO squeezer parameters (see p.70, 90 Khalaidovski thesis).

squeezer breadboard optical efficiency	93%
OPO output coupler transmission	8%
OPO intracavity loss	4%
OPO round-trip length	0.0186 m
frequency	5 MHz
OPO threshold power	60 mW

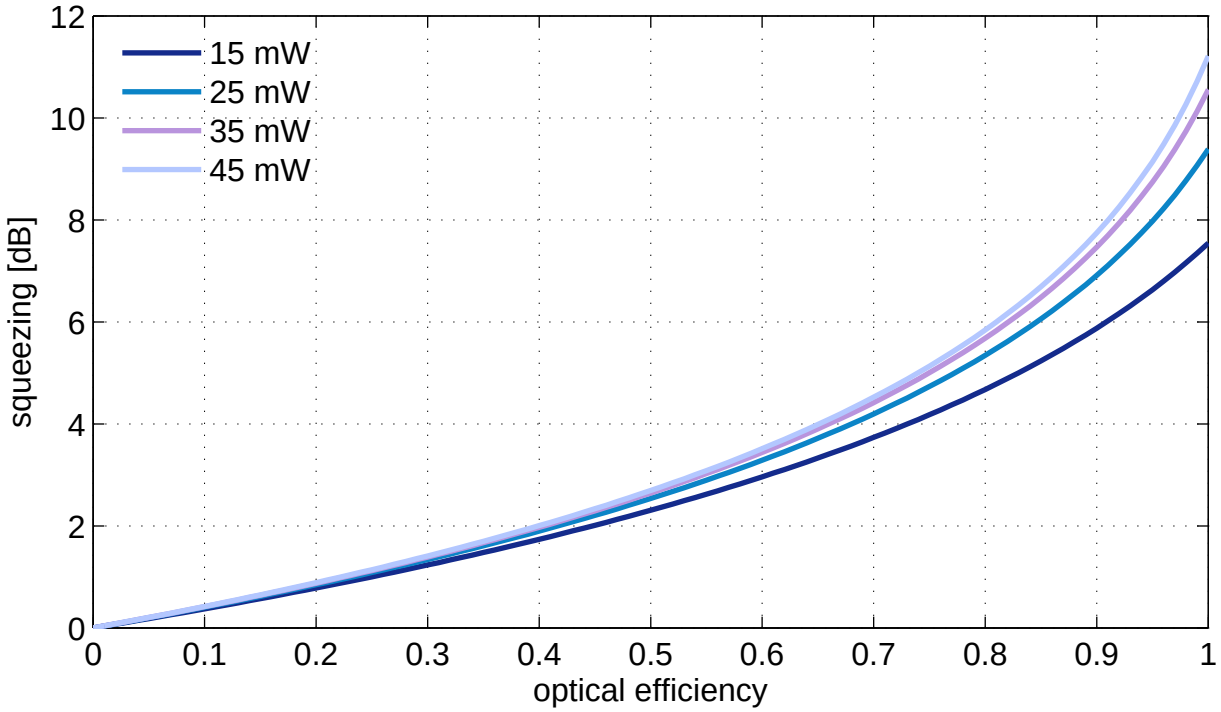

Figure 2: The expected amount of observed squeezing based on the green pump power and the optical efficiency of the squeezed field path. This model assumes no phase noise.

3.2 Optical losses

Any time the squeezed vacuum field experiences an optical loss, the lost fraction of light is replaced by the classic vacuum field:

$$V' = VT + L \tag{1}$$

Here, V is the initial variance of the squeezed state, T the optical efficiency, and L the optical losses, where $T + L = 1$. Figure 2 shows how the degree of squeezing is degraded as a function of optical efficiency for several different pump powers.

3.3 Phase noise

Phase noise arises when there is relative motion between the angle of the squeezing ellipse and the angle of the measurement quadrature of the interferometer. The degree of (anti-)squeezing is reduced to the following quantities for an rms phase noise of θ:

$$V_s' = V_s \cos^2\theta + V_a \sin^2\theta \tag{2}$$
$$V_a' = V_a \cos^2\theta + V_s \sin^2\theta \tag{3}$$

where V_a and V_s are the variances of the anti-squeezed and squeezed states, respectively, before including the effect of phase noise. Note that for small θ, the change in the (anti-

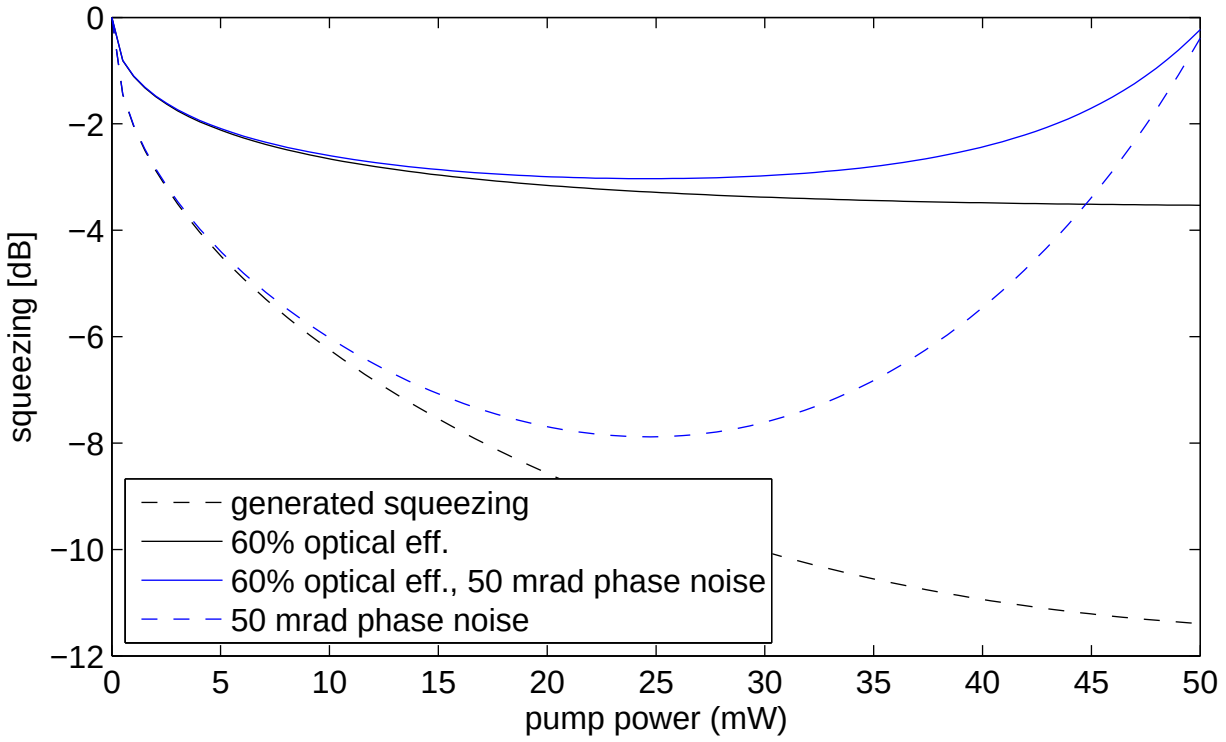

Figure 3: Generated squeezing as a function of the pump power (black dashed curve) shown in contrast with the equivalent curves that include 60% optical efficiency and 50 mrad phase noise. These numbers are selected for demonstration purposes only.

)squeezed states depends linearly on the degree of squeezing/anti-squeezing, respectively. Given the amount of anti-squeezing is much greater than the amount of squeezing (see Fig. 1), the squeezed state is much more affected by phase noise than the anti-squeezed state. Figure 3 shows how the squeezing as a function of pump power is reduced significantly at high pump powers (ie. where there are the highest levels of anti-squeezing). For example, we see in Fig 3 that the highest pump power of 45 mW is only beneficial if the total rms phase noise is less than 10 mrad. Figure 4 shows squeezing as a function of phase noise for several pump powers when the optical losses are 40%.

4 Optical losses

Table 2 summarizes GEO's optical loss budget for the squeezer path as of July 2012. We find that only 63% of the squeezed light sent into the interferometer is detected by the PD. With the nominal 35 mW pump power, or 10.5 dB injected squeezing, these optical losses alone reduce the maximum possible level of achieved squeezing to 3.7 dB.

The single greatest source of loss is the OMC and second is the detection PD. The OMC is known to have excessive losses due to poor AR coatings and most likely dirty mirrors and

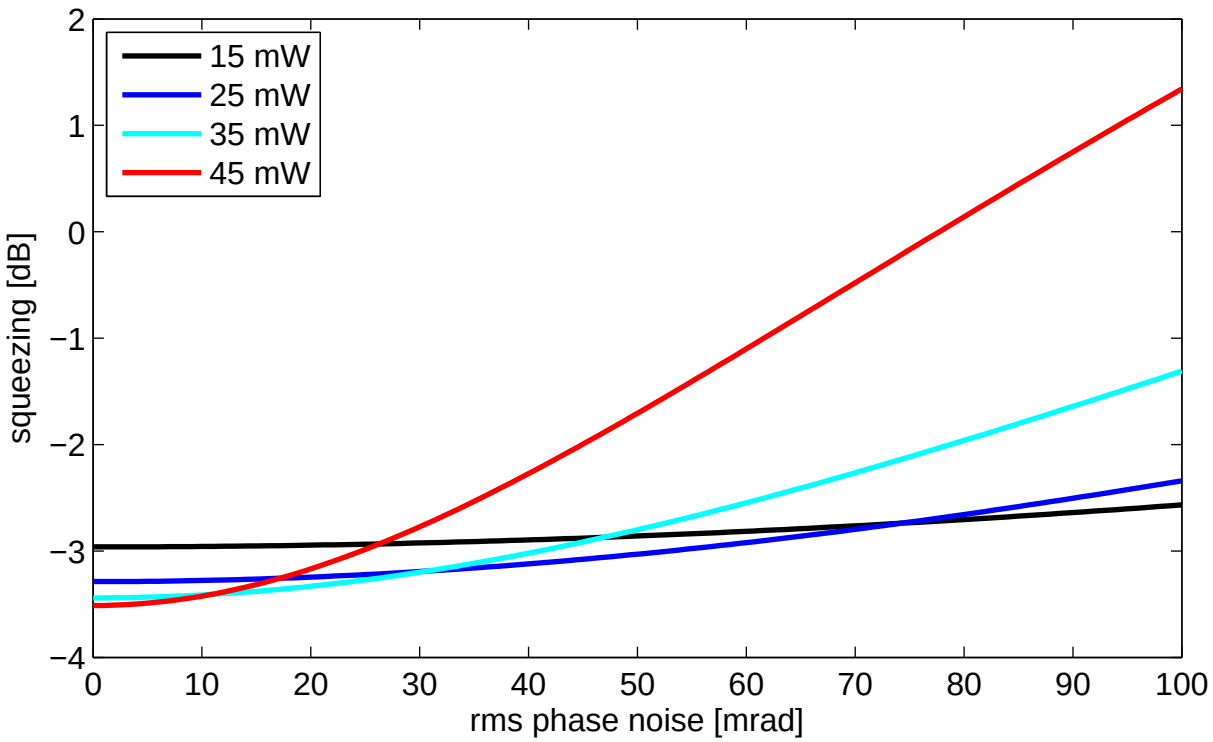

Figure 4: Observed squeezing as a function of phase noise for 4 different pump powers when optical losses are 40%.

Table 2: Optical losses of squeezed beam. The resulting transmission upon multiplying the optical efficiencies in series is 63%.

component	power loss	comment
squeezer path Faraday	3.3%	1.5%
output port Faraday	3.3% × 2	guess
BDO1 transmission	1% × 2	
SR cavity (when locked)	1%	above 1 kHz
OMC mode-matching loss	2%	
squeezer mode-matching loss	6%	
OMC AR coating loss	1%	
OMC internal losses	14%	deduced from other measurements
OMC trans PD detection loss	9%	Perkin-Elmer

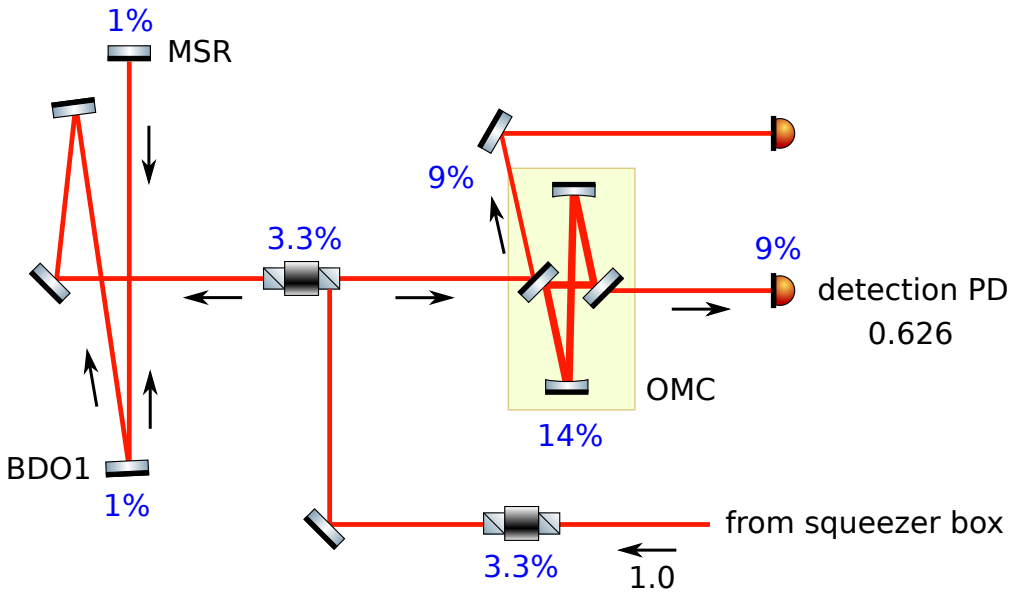

Figure 5: Optical losses in the squeezer path.

can in principle be easily improved with new optics. The current Perkin-Elmer photodiode is also a high-loss component that can be replaced with a much better specimen. The polarizing beam splitters of the Faraday isolators each have approximately 1% loss and with investigation into better polarizers, may be improved. Details of short-term goals for improvement of optical efficiency are found in Section 7.

4.1 Mode-matching

The concept of mode-matching the squeezed field to GEO's output field is to independently match the squeezed field and the GEO output field to the OMC. The mode-matching of GEO to the OMC was measured to be approximately 98% (Nov. 11, 2011 logbook entry). The mode-matching lenses that match the squeezed field to GEO's output field were selected based on a model that assumes a mirror image of the OMC waist in the squeezer injection path (I'm confused about this idea at the moment.), and then tuned in-situ. The tuning was done with the bright alignment beam with a single bounce off the signal recycling mirror. We scanned the OMC and minimized the TEM02/20 mode. The mode-matching is approximately 94% (Nov. 15, 2011 elog).

4.2 Alignment

The squeezed field needs to be aligned to the carrier field at the inteferometer output port. There are several ways of generating an alignment signal, all of which use the squeezer coherent control sidebands. The true alignment signal is the beat between the TEM00 and TEM01/10 modes of the carrier and the CCSBs. However, most of the carrier light at the output port is made of higher order modes which create a false signal. Because the

Table 3: Options for generating an alignment error signal.

where	what	frequency
OMC REFL QPD	CCSBs vs. MI RF SBs	300 kHz
FAR camera	CCSBs vs. carrier	15.2 MHz
FAR camera	CCSBs vs. MI RF SBs	300 kHz

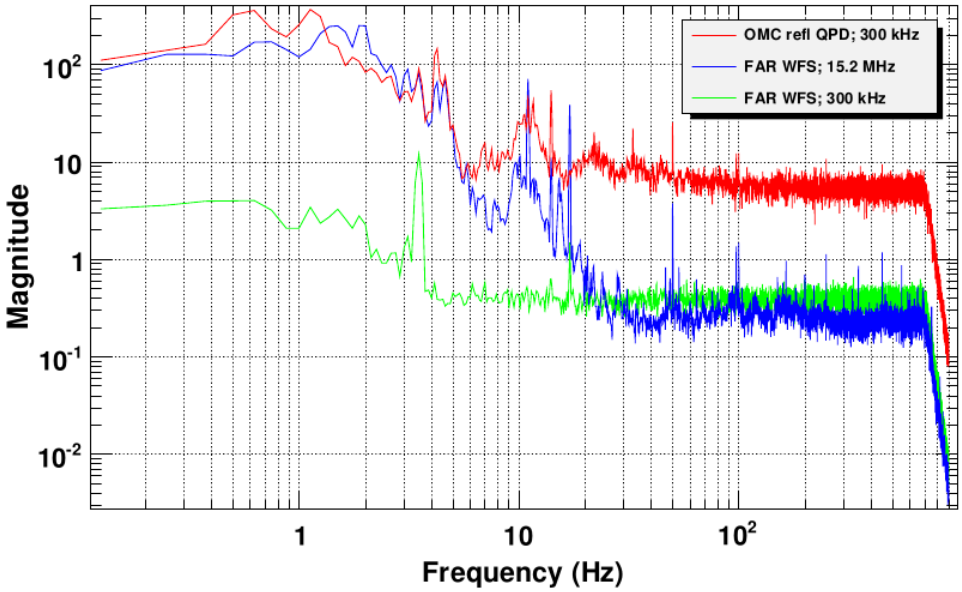

Figure 6: Comparison of three potential automatic alignment error signals.

Michelson sidebands in GEO are spatially cleaner at the output port than the carrier is (the Schnupp asymmetry means they don't see the imperfect mirrors as many times as the recycled carrier does) and should be aligned to the carrier, they serve as a potential alignment signal candidate. A summary of the options explored for generating an alignment signal are found in Table 3 and example rot (yaw) spectra are found in Figure 6.

We closed the FAR WFS rot loop (carrier vs. CCSBs) with a simple set of control filters consisting of a pole at 2 Hz and a zero at 8 Hz. The plant (the PZT) has a pole at 8 Hz. We increased the gain so the ugf was at 4 Hz. Error spectra comparing the loop open/closed are found in Figure 7. This runs successfully, but an offset in the loop is required because higher order modes of the carrier mean the optimal DC pointing is not achieved by driving the error point to zero. Whether this offset changes has not yet been studied, and an integrator needs to be added to the control filters.

5 Phase noise

The squeezing ellipse orientation must match the angle of the interferometer output field to make the best use of the squeezed field. The interferometer output field is ideally made up

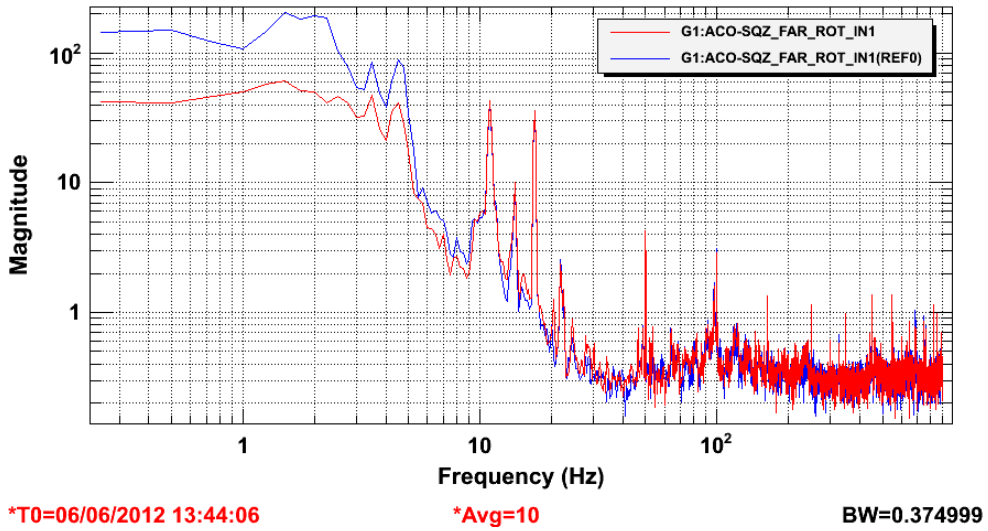

Figure 7: Example of reduction in sqz AA error point due to closed loop.

of only the local oscillator for the gravitational-wave signal, the dark fringe offset. However, in practice, other light is present and not only contributes to the shot noise at the detector, but has the potential of phase modulating the local oscillator. It should be pointed out that only the rms phase noise matters, not the shape of the frequency content.

5.1 Phase noise sensing and control

There are several options for how to implement a squeezer longitudinal phase servo. First, there are four choices for how to generate such an error signal:

1. carrier against CCSBs at pick-off before OMC
2. MI RF SBs against CCSBs at pick-off before OMC
3. MI RF SBs against CCSBs in OMC refl
4. carrier against CCSBs in OMC trans (OMC can't have too high a finesse!)

We are currently using option 3, and will soon have the electronics to test out option 4.

Second, there are choices for how to feedback a control signal:

- add to 80 MHz frequency generator used for demodulation of sqz. to GEO laser PLL loop
- PZT in the squeezer injection path

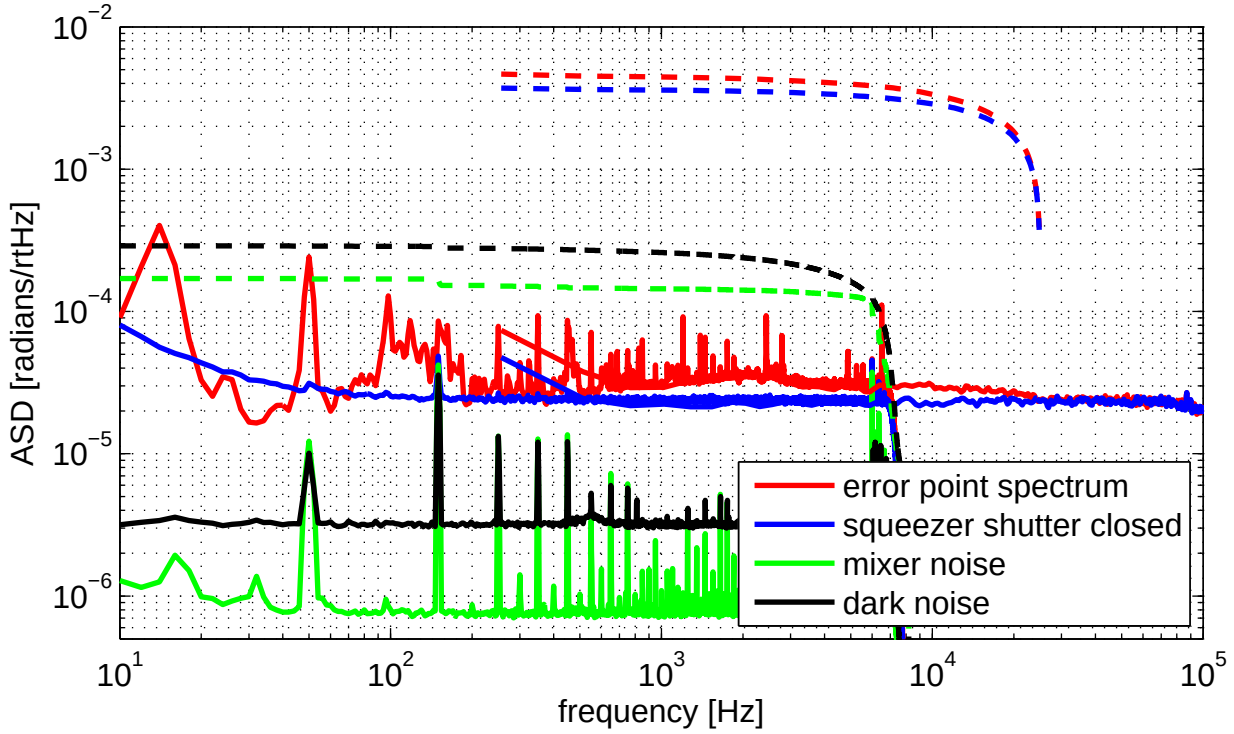

Figure 8: Calibrated squeezer phase error point (red curve), measured as the beat between the squeezer control sidebands and the RF Michelson sidebands in reflection of the OMC. This loop operates with a bandwidth of about 1 kHz and is limited by sensor/shot (blue curve) above 25 kHz. The controlled spectrum is so flat such that little to no improvement in rms noise is to be gained by increasing the gain. The servo is sensor noise limited.

Our current setup for creating a squeezer to GEO output relative phase error signal uses the beat of the squeezer sidebands with the Michelson sidebands in reflection of the OMC which are at 15.2 MHz and 14.9 MHz, respectively. We feed back to the summing junction of the 80 MHz frequency generator. We also inject a line at 6500 Hz to calibrate the error signal. The measured residual phase noise is 5 mrad as seen in Figure 8. (We need to verify the calibration.)

5.2 Noiselock

We implement a slow servo called the *noiselock loop* that serves to change the squeezing quadrature in order to maximize the strain sensitivity. The demodulation phase of the longitudinal phase error signal is dithered at 11.6 Hz and a band-limited root-mean-square of strain is then demodulated at this dither frequency and a control signal derived. A schematic of the servo is in Figure 9. The underlying causes for slow phase drift is not understood at this time. An example of how much drift we observe is shown in Figure 10.

(I need to explain why dithering the demod phase shifts the squeezing phase. E.g. the

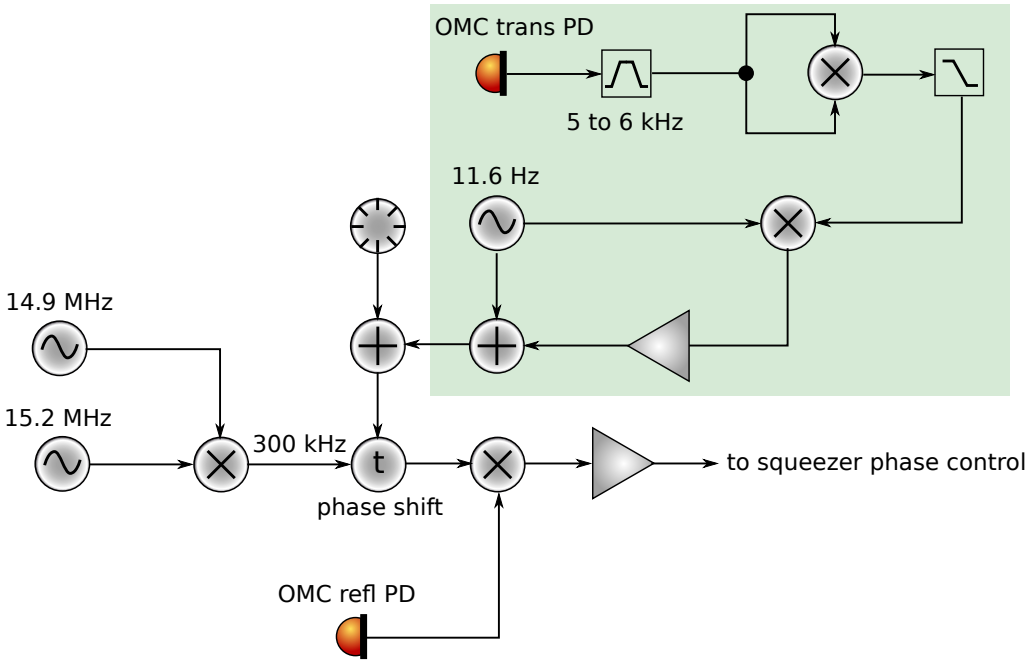

Figure 9: Schematic of the noiselock servo. The demodulation phase of the squeezing angle error signal is modulated at $f_0 = 11.6$ Hz. The band-limited rms of interferometer strain is in turn demodulated at f_0 and a derived control signal is in turn sent to the demodulation phase of the squeezing angle error signal.

CCSBs are unequal in amplitude, making the locking point at some offset from 0.)

5.3 RF frequencies

This section is based on work from LIGO T0900325 and evaluates the role of the RF sidebands in generating phase jitter of the interferometer output field. Understanding the phase noise contribution from the RF sidebands is important both because the contribution can be large and because the squeezing ellipse orientation cannot follow at these frequencies. Phase noise due to the RF sidebands may, however, be reduced, as will be discussed shortly.

The dominant fields at the interferometer output port are those from the dark fringe offset, the contrast defect, and the RF sidebands. The dark fringe offset is the local oscillator for the gravitational-wave sidebands in a DC readout configuration and is generated by holding the Michelson arms slightly off of the dark fringe at the anti-symmetric port. The contrast defect is light that makes it to the anti-symmetric port due to asymmetry in the reflectivity of each Michelson arm. The RF sidebands are ideally filtered by the OMC, but due to limited finesse, some percentage is transmitted.

One of two effects of the RF sidebands on phase jitter comes from the fact that the Michelson interferometer rotates the differential carrier field by 90°, but leaves all other fields the same

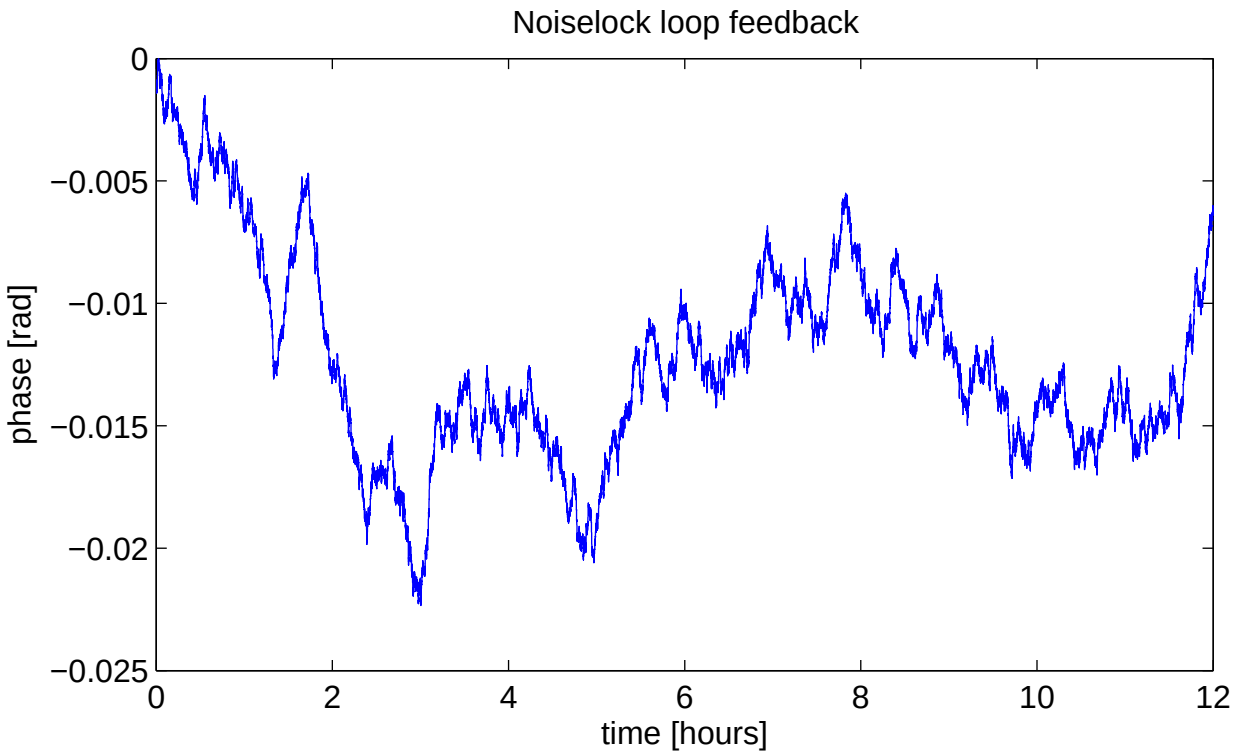

Figure 10: Example of drift of squeezer demodulation phase over the course of 12 hours.

(including the RF sidebands and the contrast defect). The result is that at the output port, as shown in Figure 11, the RF sidebands are amplitude modulation (AM) of the dark fringe offset, yet continue to be phase modulation (PM) of the contrast defect.

Because the squeezing quadrature is determined by the sum of the fields at the interferometer output, both AM of the dark fringe offset and PM of the contrast defect affect the angle that the squeezing ellipse orientation must be matched to. Figure 12 shows phasors depicting these two situations. Should the ratio of dark fringe offset to contrast defect amplitude be large, these effects are reduced.

The second effect of the RF sidebands on phase jitter arises when the upper and lower sidebands are unequal in amplitude. Rather than produce pure AM on the DFO and PM on the CD, there is some component of PM on the DFO and AM on the CD.

In summary, changes in the interferometer output phase at RF frequencies are created in four ways:

- phase noise of the contrast defect
- amplitude noise of the dark fringe offset
- phase noise of the dark fringe offset due to unequal RF sideband amplitudes
- amplitude noise of the contrast defect due to unequal RF sideband amplitudes (true?)

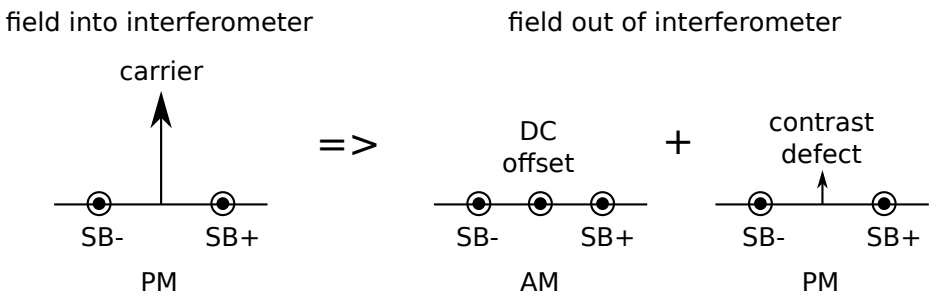

Figure 11: The RF sidebands (SB+ and SB-) are generated via phase modulation of the carrier field. The Michelson interferometer rotates the differential carrier field by 90°, but leaves all other fields the same, including the RF sidebands and the contrast defect. The result is that at the output port, the RF sidebands are amplitude modulation (AM) of the dark fringe offset, yet continue to be phase modulation (PM) of the contrast defect.

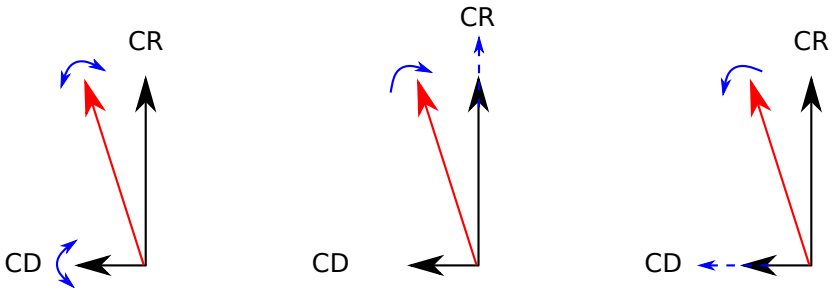

Figure 12: Examples of how jitter of the squeezing quadrature is generated. replace!

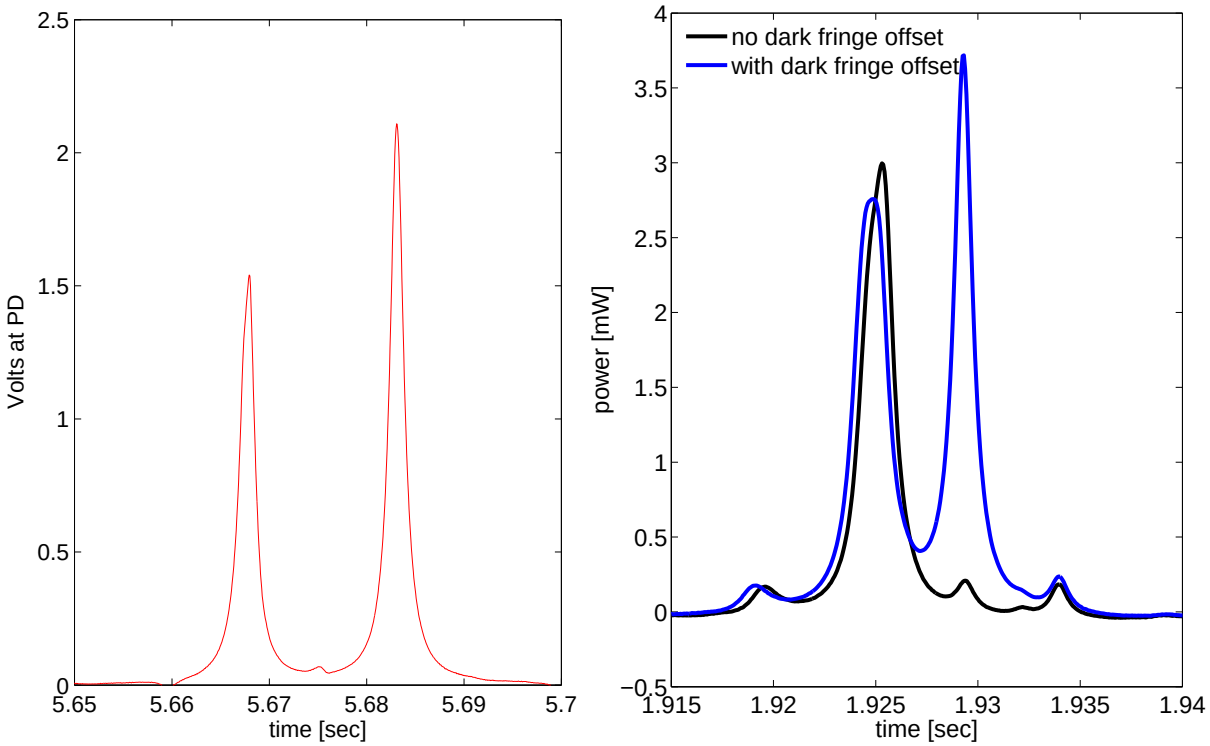

Figure 13: Mode scan of the output port. The left-hand plot shows the Michelson RF sideband imbalance. A higher-order carrier mode sits on top of the lower sideband, so this figure is created by subtracting the carrier content. The imbalance is $\epsilon = 0.06$. The right-hand plot shows the ratio of contrast defect to carrier power for our typical dark fringe offset. The ratio is about 0.05. The sideband amplitude is reduced by a factor of 4.4 from fall 2011 and is the new standard.

and may be expressed mathematically as in Eq. 90 from T0900325:

$$\Gamma_{\rm rms} = \sqrt{\frac{P_{\rm SB}}{P_{\rm CR}}\left(\frac{1}{\eta} + \epsilon^2\frac{\eta - 1}{\eta}\right)} \tag{4}$$

All powers in this equation are for those transmitted through the OMC, and the variables η and ϵ are defined as follows:

$$\eta = \frac{P_{\rm CR}}{P_{\rm CD}} \tag{5}$$

$$\epsilon = \frac{1}{2}\frac{P_{\rm SB+} - P_{\rm SB-}}{P_{\rm SB+} + P_{\rm SB-}} \tag{6}$$

The sideband imbalance is quantified by ϵ and a sample measurement of the imbalance is shown in Figure 13a. Currently, $\epsilon = 0.06$. The contrast defect, commonly quoted as $1/\eta$, can be measured by comparing the power transmitted through the OMC with and without the dark fringe offset. It accounts for approximately 5% of the power at the output port, as seen in Figure 13b.

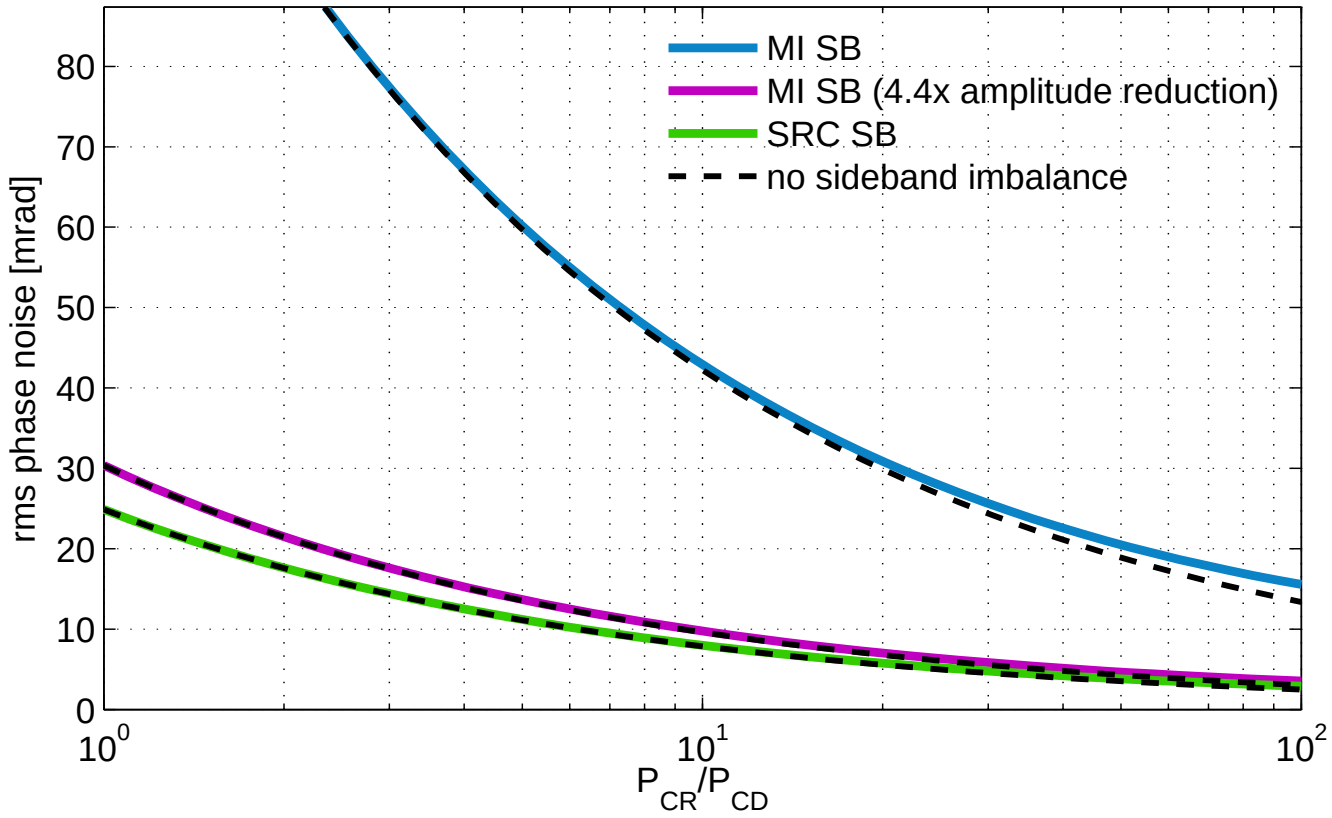

Figure 14: RMS phase noise as a function of the ratio of DC offset light to contrast defect light in the OMC transmitted beam. The typical operating point for GEO is $P_{\rm CR}/P_{\rm CD} = 20$, which corresponds to an RMS phase noise for the Michelson sidebands of 6.7 mrad and 5.5 mrad for the SRC sidebands. The quadrature sum is 8.7 mrad.

Figure 14 shows the dependence of phase noise on contrast defect for our current sideband imbalance. This uses $P_{CR} = 1.6$ and $P_{MI\_SB+} = 0.08 T_{MI}$ (for the 4.4× sideband amplitude reduction). We estimate the signal recycling cavity sideband amplitude as $P_{SR\_SB+} = 0.02 T_{SC}$. Note T_{MI} and T_{SR} are calculated in Table 6. We explored the effect of these factors on observed squeezing by changing the rms phase noise up to a factor of 4.4 by reducing the sideband amplitude. We also tried increasing the dark fringe offset.

5.4 Higher order modes

Role?

5.5 Total known phase noise

Taking the measured and anticipated rms phase noises at different frequencies and adding them incoherently, we find that we have a total known phase noise of 10 mrad rms. The

Table 4: Measured and calculated phase noises. The quadrature sum is 10 mrad rms.

source	rms phase [mrad]
error point	5
14.9 MHz sidebands	6.7
9 MHz sidebands	5.5

summary of phase noises is shown in Table 4.

5.5.1 Measuring total phase noise

We currently do not have information about the rms phase noise between audio and RF frequencies. We can indirectly determine what it is by measuring the total phase noise via its effect on the observed squeezing level. We can measure the total rms phase noise by mapping out the curve of Figure 3. However, this will be difficult if the total phase noise happens to be very small ($\leq$ 10 mrad) because then the effect of phase noise is only measurable at very high pump powers. At the moment, we are limited to at most approximately 35 mW pump power (the MZ won't lock when we request more than that) and we know of only approximately 10 mrad phase noise. A method of putting an upper limit on the total phase noise is to purposefully increase it by a known amount (i.e. keep amplitude of MI RF sidebands at a higher level) and measure the squeezing versus pump power curve. A first set of measurements are shown in Figure 15. Our optical loss budget predicts only 40% losses and our known phase noises amount to 10 mrad, but this data is more consistent with 50% optical losses and 70 mrad phase noise.

6 Expected observed squeezing

Based on our measurements of the optical losses and phase noise, we can predict the best possible achieveable squeezing level to be observed with GEO. With a green pump power of about 17 mW such that the injected squeezing level is 8 dB and with 37% losses, the best squeezing possible is 3.2 dB. Phase noise of 10 mrad has a negligible effect. As of early March, we measured 2.9 dB, leaving a 0.3 dB gap, which in fact is explained by other contributing noise sources at high frequencies such as dark noise and laser amplitude noise (present these as a standard noise source). Figure 16 shows an example of these other noise levels as of mid-April. This full accounting of observed squeezing is not always realized, however. Since mid-April, for example, there remains a gap.

7 Ideas for improvements

1. better OMC

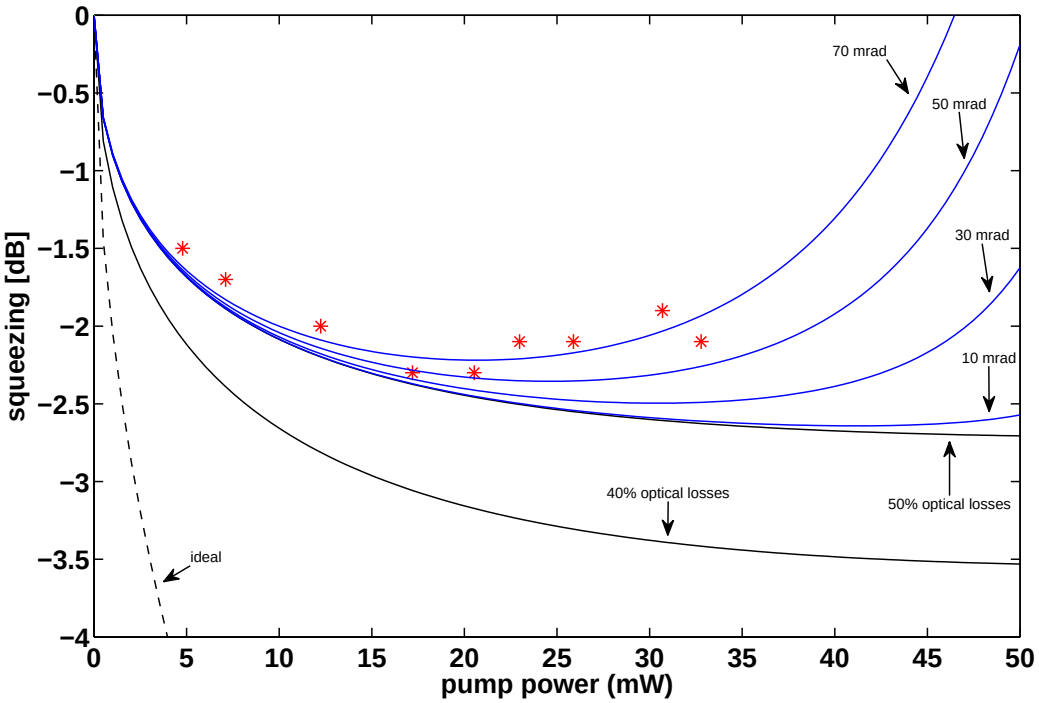

Figure 15: First look at a measurement of squeezing vs. pump power.

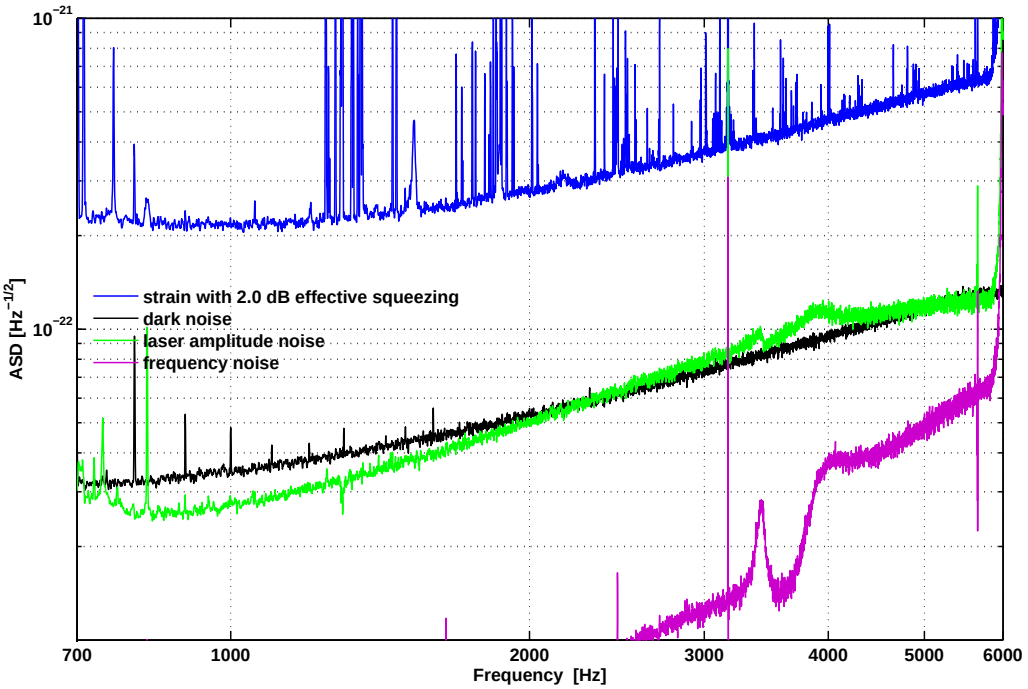

Figure 16: High frequency noises that result in a lower effective squeezing of strain than is actually achieved. In this example, shot noise is actually reduced by 2.4 dB due to squeezing, but the other noise sources, when added in quadrature with shot noise, reduce the effective squeezing to 2.0 dB. In this example, laser amplitude noise is abnormally high. (show more recent noisebudget)

Table 5: Optical losses of squeezed beam.

component	power loss	6-month goal
squeezer path Faraday	3.3%	1.5%
output port Faraday	3.3% × 2	1.5% × 2
BDO1 transmission	1% × 2	1% × 2
SR cavity (when locked)	1%	1%
OMC mode-matching loss	2%	2%
squeezer mode-matching loss	6%	2%
OMC AR coating loss	1%	0.1%
OMC internal losses	14%	5%
OMC trans PD detection loss	9%	3%

Table 6: OMC parameters. Many numbers come from p.12 of the GEO-HF logbook.

quantity	symbol	value	units
Finesse	F	160	
round trip length	L	0.658	m
g-factor	g	0.735	
waist size	ω_0	450	µm
free spectral range	FSR	455.6	MHz
Michelson sideband frequency	f_{MI}	14.90	MHz
SRC sideband frequency	f_{SR}	9.18	MHz
Michelson sideband power transmission	T_{MI}	1.01	%
SRC sideband power transmission	T_{SR}	2.71	%

2. 2 PDs to have constant monitor of level of shot noise reduction (sum vs. difference)

3. 2nd OMC

8 Acknowledgements

9 Appendix–OMC

Table 6 summarizes the current output mode cleaner (OMC) design parameters. Note that the sideband transmission numbers (T_{MI} and T_{SR}) should be doubled in practice to account for the existence of both upper and lower sidebands.